Experimental and Computational Examination of the Coandă Effect on the Space Launch System at Liftoff Conditions

T.J. Wignall,* Morgan A. Walker,† and Jesse G. Collins‡
NASA Langley Research Center, Hampton, VA 23681

During development of an aerodynamic database to cover ground wind loads, uncertainty quantification to account for the Coandă effect forced a closer look into how this phenomenon manifests on the Space Launch System. Aerodynamic data collected across the life of the program are explored to look for trends and the ability to characterize not just the bounds of forces and moments but also better understand their distributions. Experimental data collected in the NASA Langley 14- by 22-Foot Subsonic Tunnel are used to explore integrated forces and moments. This is followed up by a similar exploration using computational data generated using the Kestrel flow solver. After a survey of the data at large, which confirms the existence of the Coandă states throughout the history of the program, a few highlighted cases are used to characterize the flow physics. This characterization is used to summarize how each Coandă state is predicted to load the vehicle.

Nomenclature

LSRB	=	Left Solid Rocket Booster
ML	=	Mobile Launcher
RSRB	=	Right Solid Rocket Booster
SLS	=	Space Launch System
SRB	=	Solid Rocket Booster
State SB	=	State Symmetric Booster (Flow attaches to SRB on both sides)
State SC	=	State Symmetric Centerbody (Flow attaches to centerbody on both sides)
State AL	=	State Asymmetric Left (Flow attaches to the left)
State AR	=	State Asymmetric Right (Flow attaches to the right)
C_p	=	Pressure coefficient
C_f	=	Magnitude of skin friction coefficient
$\hat{C}_A$	=	Normalized axial force coefficient
$\hat{C}_N$	=	Normalized normal force coefficient
$\hat{C}_Y$	=	Normalized side force coefficient
$\Delta\hat{C}_N/\Delta\hat{x}$	=	Normalized normal force lineload
$\Delta\hat{C}_Y/\Delta\hat{x}$	=	Normalized side force lineload
$\hat{C}_l$	=	Normalized rolling moment coefficient
$\hat{C}_m$	=	Normalized pitching moment coefficient
$\hat{C}_n$	=	Normalized yawing moment coefficient
h/L	=	Height of the vehicle above the ML pad normalized by height of ML
α_P	=	Total angle of attack, missile axis [degrees]
ϕ_P	=	Roll angle, missile axis [degrees]

*Research Aerospace Engineer, Configuration Aerodynamics Branch, thomas.j.wignall@nasa.gov
†Research Aerospace Engineer, Configuration Aerodynamics Branch, AIAA Member.
‡Research Aerospace Engineer, Configuration Aerodynamics Branch, AIAA Member

I. Introduction

As part of the Space Launch System (SLS) program, which will be used for the Artemis missions to return astronauts to the Moon, the SLS Aerodynamics Task Team is responsible for analysis of the aerodynamic environment from prelaunch until the rocket leaves the atmosphere. During recent development of databases designed to characterize aerodynamic loading from ground winds while the vehicle is on the launch pad, relatively large uncertainties in side force where established. These can be traced back to the Coandă effect as observed during wind tunnel testing as explored in Ref. [1]. This paper takes the next step by expanding analysis away from a single wind tunnel test and looking at collected results across the history of the SLS program with the eventual goal of characterizing the multimodal states due to the Coandă effect on the SLS and similar three cylinder geometries.

The ground wind loads database that led to this analysis is broken into a distributed loading portion and an integrated force and moment portion, which guided the analysis here. This paper starts by looking for trends in the collected wind tunnel data across four different tests with a focus of identifying if all possible Coandă states are observed. A secondary focus is to see if there are any patterns that can be used to predict which state is likely to be experienced by the Artemis I launch vehicle and beyond. From there, exploration continues by examining the computational data generated across several geometries and versions of the CREATE-AV Kestrel CFD solver. A similar analysis as conducted for the wind tunnel is performed but with the distributed lineloads that come out of CFD.

After global trends are examined for confirmation of the Coandă state existing across configurations and analysis tools, a more in-depth analysis is done. This analysis focuses on using CFD to explore the interaction of the flow phenomenon and surface data. Lineloads are then used to show how those surface features translate to forces and moments of interest. This analysis is used to characterize the predicted forces of each Coandă state.

A. SLS and the Ground Wind Loads Database

The SLS refers to a series of heavy-lift launch vehicles that are designed for deep space exploration missions such as the Artemis program. There are three classes of SLS configurations with crew and cargo variations as seen in Fig. 1 for a total of six main configurations. The Block 1 and Block 1B configurations have been the focus of the SLS program so far and will be the configurations analyzed in this paper. As the program has evolved, changes have been made to the geometry and there have been several versions of each configuration. Since this paper uses data collected over the history of the program, several versions of these will be used where available and be referenced by their configuration numbers where assigned. The Block 1 Crew configurations are assigned numbers of the form SLS-1000X where X represents the version number. The Block 1 Cargo configurations are assigned numbers of the form SLS-1050X while the Block 1B Cargo and Crew are SLS-2700X and SLS-2800X, respectively. There is one variation of the Block 1 Cargo that was tested but not assigned a formal version number and will be referred to SLS B1 Cargo sCPLF. The SLS vehicles are made of many components, but since this work is about the aerodynamics of the Coandă effect the focus will be on the core stage, which makes up the lower portion of the centerbody, and the two solid rocket boosters (SRBs). These three components are identical across the Block 1 and Block 1B configurations and have remained relatively unchanged since initial designs due to the use of shuttle heritage parts in their construction. This commonality in design and since only freestream flow conditions in the plane perpendicular to the vehicle centerline are being studied, allows for pooling data across configurations and for direct comparison of SRB forces and moments.

The coordinate system for the SLS program is defined in SLS-SPEC-048 ([3]), the relevant definition of aerodynamic forces and moments is reproduced in Fig. 2. Due to the wide variety of wind angles possible in the early stages of flight, total angle of attack, α_P, and roll angle, ϕ_P, are used to define the incoming wind direction. When the vehicle is in proximity to the Mobile Launcher (ML), it is useful to introduce another parameter, height above the pad, which is normalized by the height of the ML, h/L. Figure 3 shows a graphical representation of the definition of h/L as well as contextual reference for ϕ_P while the vehicle is adjacent to the ML. While both a missile axis and a body axis are defined, all forces and moments shown in this paper will be in body axis. This is partially because most of the analysis is focused on a single condition, but also, to prevent confusion on the directionality of forces. For this paper the analysis is focused on $\alpha_P = 90°$, $\phi_P = 180°$. When the SLS is on the ML, this corresponds to winds coming from the South. Conveniently when looking at the vehicle from the South at this condition, the Right SRB (RSRB) is on the right (or East) side of the vehicle, and the Left SRB (LSRB) is on the left (or West) side of the vehicle. This becomes important as the proposed Coandă states are defined in terms of left and right.

This paper is a direct result of work in support of aerodynamic databases that characterize the prelaunch aerodynamic loading due to ground winds. The ground wind loads databases characterize resulting aerodynamic forces on both the ML and the SLS as a result of flow from any wind direction. The database is split into a distributed loads sec-

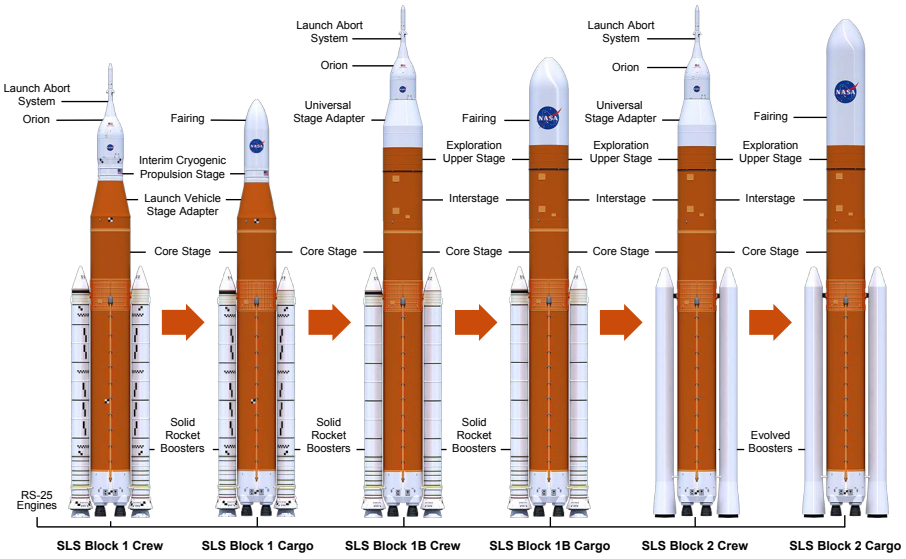

Fig. 1 The six main vehicle configurations of the SLS family [2].

tion and an integrated loads section, which means characterizing both is important and why the analysis makes heavy use of both computational and experimental data. While creating this database for the Block 1B Crew vehicle, the uncertainties that were developed using established methods fell short while trying to provide reasonable procedures to handle multimodal flow. In particular, trying to cover the range of possible side force values at $\phi_P = 180°$ to account for the Coandă effect meant a detailed analysis into the theoretically possible and observed states and their effect on loading was needed.

B. Coandă Effect

Throughout the SLS aerodynamic development cycle, force and moment discrepancies between repeat runs at the same condition were observed for a variety of different SLS configurations in the liftoff phase of testing. The discrepancies often occurred at $\phi_P = 0°$ and 180°. When the ML is included in the tunnel or simulations, $\phi_P = 0°$ no longer shows characteristics of this variation due to the blockage effects of the ML. Both computational [4, 5] and experimental [1] studies of this behavior led to the current working theory that these discrepancies originate as a result of the Coandă effect acting in the gaps between each SRB and the rocket centerbody. The Coandă effect is characterized by the tendency of a jet of fluid to attach itself to a curved surface [6]. When passing through each gap, the flow forms a jet that attaches either to the rocket centerbody or the respective SRB, yielding a total of two bistable flow states, or four different states in total, at the conditions in question.

A graphic of each of the possible Coandă states is shown in Figure 4. State symmetric centerbody (SC) corresponds to a symmetric attachment to the rocket centerbody through both gaps, state symmetric booster (SB) corresponds to a symmetric attachment to each SRB through both gaps, while states asymmetric left (AL) and asymmetric right (AR) correspond to an asymmetric attachment on the core and each of the SRBs (left and right), respectively. While the Coandă effect is present at $\phi_P = 0°$, which would swap left and right, while in operation, the ML will be between the wind and the vehicle. As a result, characterizing the Coandă effect with winds from the North is not a programmatic priority and using left and right will not cause confusion in practice.

C. Data Sources

There are two major sources of data used for this analysis. The first is a collection of CFD data used for analysis of the liftoff and transition regime of SLS. The second is the collection of wind tunnel data generated by the SLS program in the same regime. For the CFD, the data were all generated using Create-AV's Kestrel solver over several years and multiple versions of the code. A brief overview of computational methodology is given, but the main focus of the section though will be a description of what data is used in this analysis. The wind tunnel data were collected in the

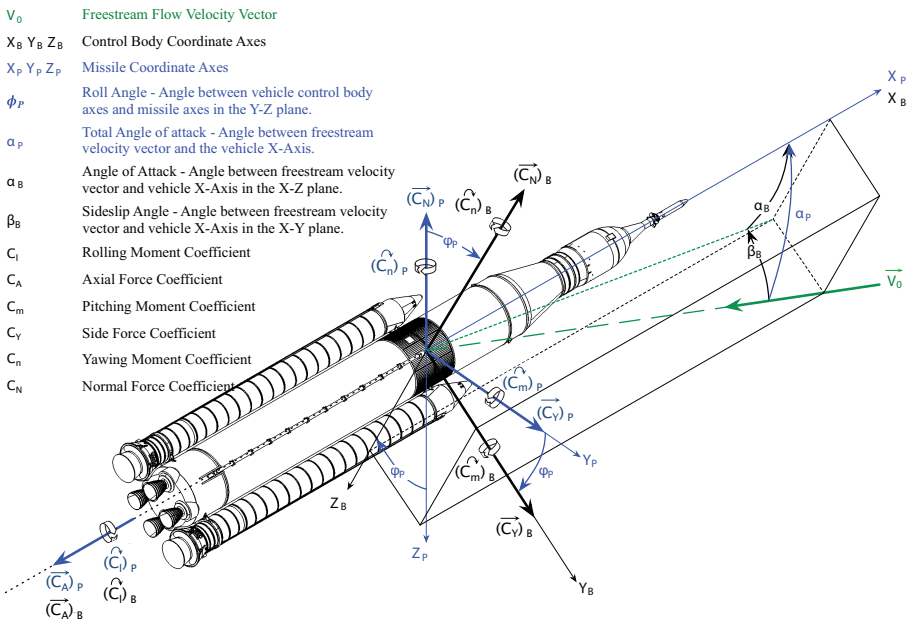

Fig. 2 SLS coordinate system for aerodynamic forces and moments [3].

NASA Langley 14- by 22-Foot Subsonic Tunnel across several tests [8–10].

All data presented in this work are in the body axis as mentioned previously. To allow for the release of this analysis to the largest possible audience, absolute scales are not used. Where possible, data normalization are done to force the primary data of interest to have values between -1 and 1. For example, all forces are normalized such that SRB side force falls between -1 and 1. For quantities where it is not possible to normalize, such as C_p, the bounds on presented scales are left off. These limitations in the presentation of the data do not take away from the meaningful technical content and discussion.

1. Computational Data

Computational data are generated using the CREATE-AV Kestrel fluid dynamic solver [11–14]. It is a finite volume, cell centered unstructured grid solver that can be coupled with a Cartesian grid solver in order to solve large problems by having an unstructured near body grid coupled with a Cartesian off body grid. Adaptive mesh refinement can then be applied to the Cartesian grid to help tackle large dynamic problems like SLS at liftoff conditions. The flow is treated as fully turbulent and the SA+IDDES scheme is used, and the grid is adapted based on the magnitude of vorticity. While solved time accurately, the data used in this analysis are time averaged over several thousand time steps. A more detailed account of computational methodology can be found in previously published work [4, 5, 7, 15, 16]. While computational techniques have been modified over time and the results used in this analysis come from multiple different versions of Kestrel, the fundamental methodology has remained constant.

2. Experimental Data

The data presented in this analysis were derived from four different wind tunnel tests of the SLS in the 14- by 22-Foot Subsonic Tunnel over a period of eight years [8–10]. A diagram of the test section and tunnel are shown in Fig. 5. While the exact configurations and experimental setups varied, each test included multiple versions of the SLS and ML mounted to a floor turntable to simulate the liftoff phase of testing. Each of the four tests included a balance to collect global force and moment measurements on the launch vehicle, while Tests 633, 648, and 657 included the addition of two load cells in each SRB that were used to collect individual SRB force and moment measurements. An example view of the liftoff experimental setup for each test is shown in Fig. 6.

The wind tunnel models are designed to take advantage of the commonality between SLS configurations. The lower portion of the vehicle is constructed in such a way that the upper portion can be swapped out depending on

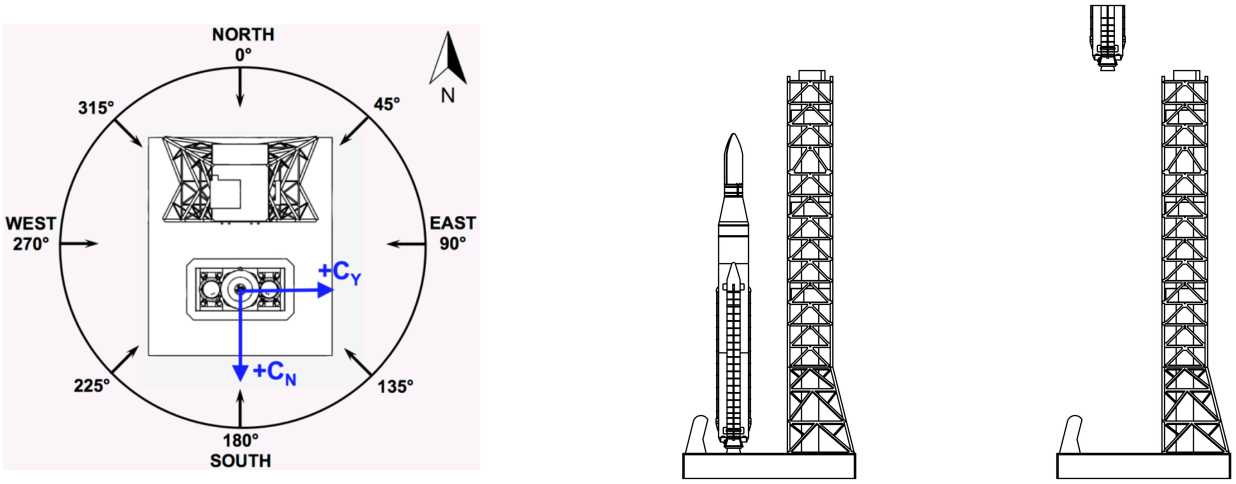

(a) Coordinate system with ML **(b) $h/L = 0$** **(c) $h/L = 1$**

Fig. 3 The SLS coordinate system in proximity to the ML showing a) definition of ϕ_P as well as direction of C_N and C_Y, b) vehicle on the pad corresponding to $h/L = 0$, c) vehicle at the top of the ML corresponding to $h/L = 1$

what configuration is to be tested. This means that the geometry where the Coandă effect manifests is identical across configurations and tests. However, these tests apply grit to the model to trip the boundary layer flow to turbulence. This grit is applied at the beginning of each test and removed after testing is complete. While this process is as identical as possible between tests, checkouts focus on uniformity across the model and similar density of grit application between tests. Local grit application in the critical region of the gap between the SRBs and the centerbody is likely to be different between tests but the commonality of the lower portion of the model means it is identical between configurations within a test. As the wind tunnel dataset is explored focusing on finding evidence of the four Coandă states, there is some evidence that this grit application influences which states are observed in a given test.

II. Observations Across Program History

As discussed previously, there have been observations that have been attributed to the Coandă effect across the SLS program but little effort to try to characterize it. The first part of characterizing this phenomenon is surveying the collected data across the program history. Wind tunnel integrated forces and moments are first explored to determine what trends exist across vehicles and tests on the integrated forces. This is followed by examining the computational data for similar trends on the lineloads.

A. Wind Tunnel Cross-Test Comparison

To determine if the presence of the Coandă effect varied between wind tunnel tests and between SLS configurations, all data at a representative condition where the Coandă effect occurred most frequently were plotted. All data points are presented without the ML in the tunnel, $\phi_p = 180°$, $h/L = 0$, and $q_\infty = 50$ psf. These data are calculated by time-averaging forces and moments over 8 seconds. As the data are explored, there are some points that do not fall into the expected states. Without digging into the time accurate data, it is impossible to say if these data represent points where the Coandă state flips over that 8 seconds window or if there is a stable "partial" state where flow is not attached fully to either the SRB or the centerbody. The results for the total vehicle balance are shown in Fig. 7.

Test 657 shows the strongest evidence toward the presence of bistable flow states on the SLS. As discussed in Ref. [1], this is the test where the variations in Coandă state during repeats were detected, which drove the decision to gather more data in an attempt to characterize it. This is most apparent in side force $\hat{C}_Y$, yawing moment $\hat{C}_n$, and rolling moment $\hat{C}_l$, where two very clear clusters are present for each of the configurations run in Test 657. Normal force $\hat{C}_N$ shows much less of a bistable scatter, which was also expected based on previous observations of the data.

Looking at the other tests and configurations, bistable states appear to be present in Test 648 across the tested configurations as well; however, one of these states appear to be different than states seen in Test 657. It is difficult

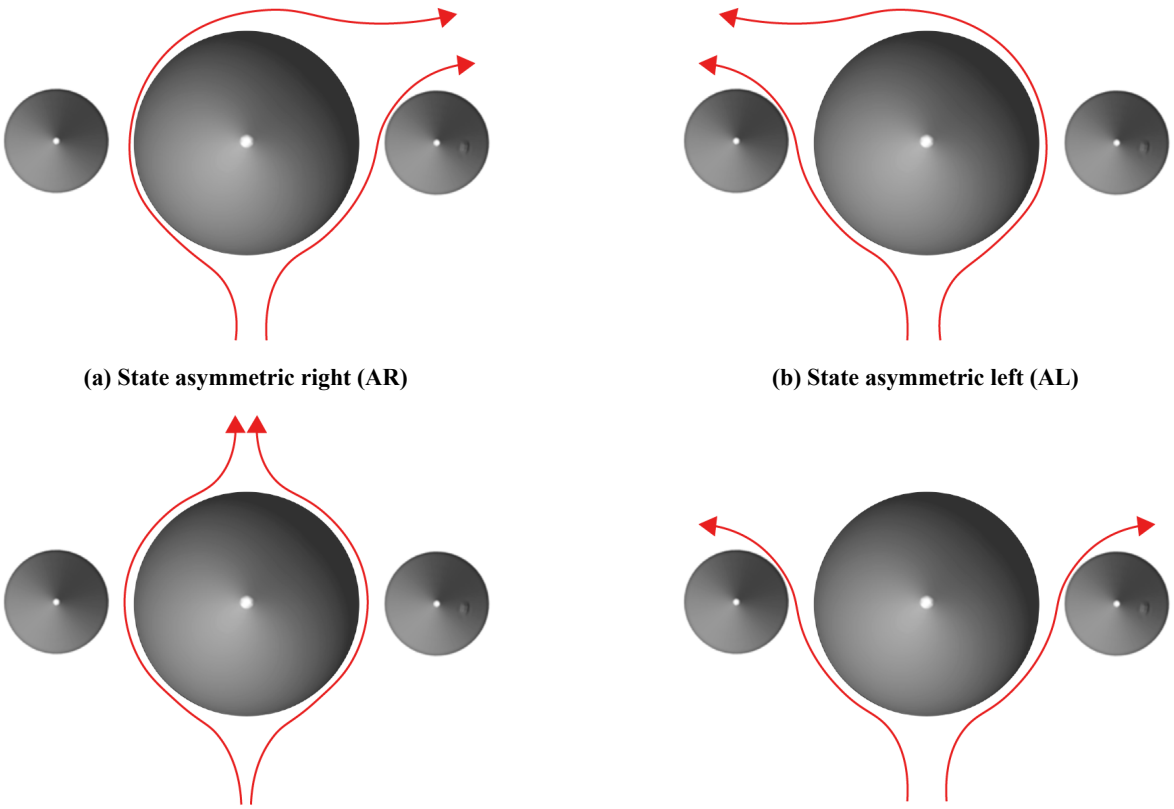

(a) State asymmetric right (AR)

(b) State asymmetric left (AL)

(c) State symmetric centerbody (SC)

(d) State symmetric booster (SB)

Fig. 4 Streamline traces of potential flow states at $\phi_P = 180^\circ$ (winds from the South) [7]. (a) State asymmetric right (AR), flow attached to the rocket centerbody and RSRB, (b) State asymmetric left (AL), flow attached to the rocket centerbody and LSRB, (c) state symmetric centerbody (SC), flow attached to the rocket centerbody alone, and (d) state symmetric booster (SB), flow attached to the RSRB and LSRB.

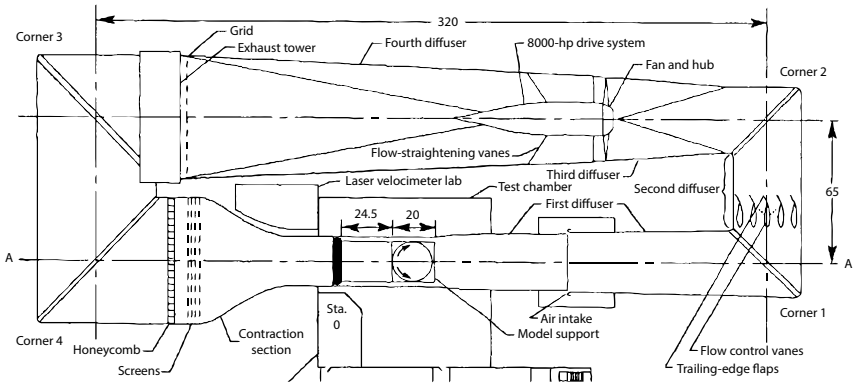

Fig. 5 Plan view of the NASA Langley 14- by 22-Foot Subsonic Tunnel [17]. Dimensions are in feet.

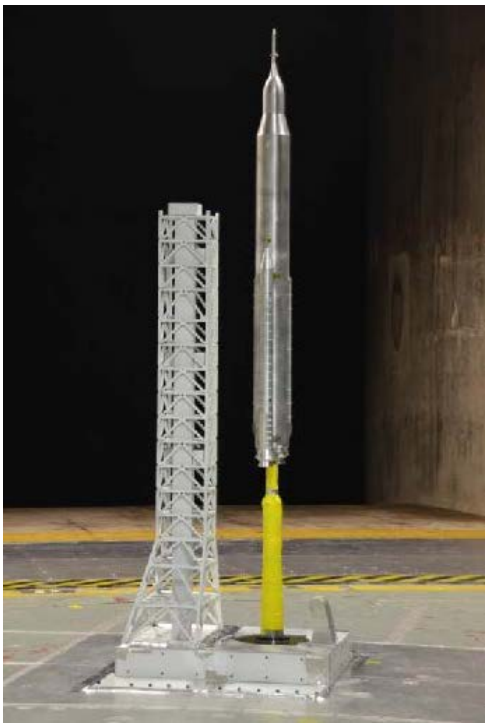

(a) Test 609, SLS Block 1B Crew with old ML-1

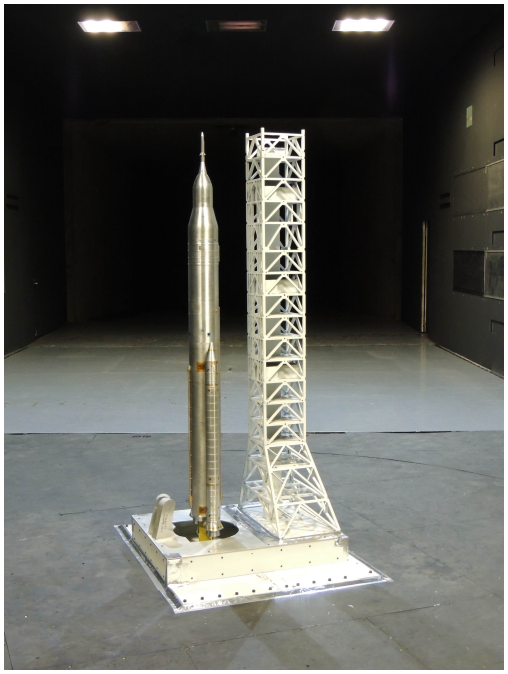

(b) Test 633, SLS Block 1B Crew with ML-1E

(c) Test 648, SLS Block 1 Crew with new ML-1

(d) Test 657, SLS Block 1B Cargo with ML-2

Fig. 6 Liftoff phase experimental setup for various SLS tests in the 14- by 22-Foot Subsonic Wind Tunnel.

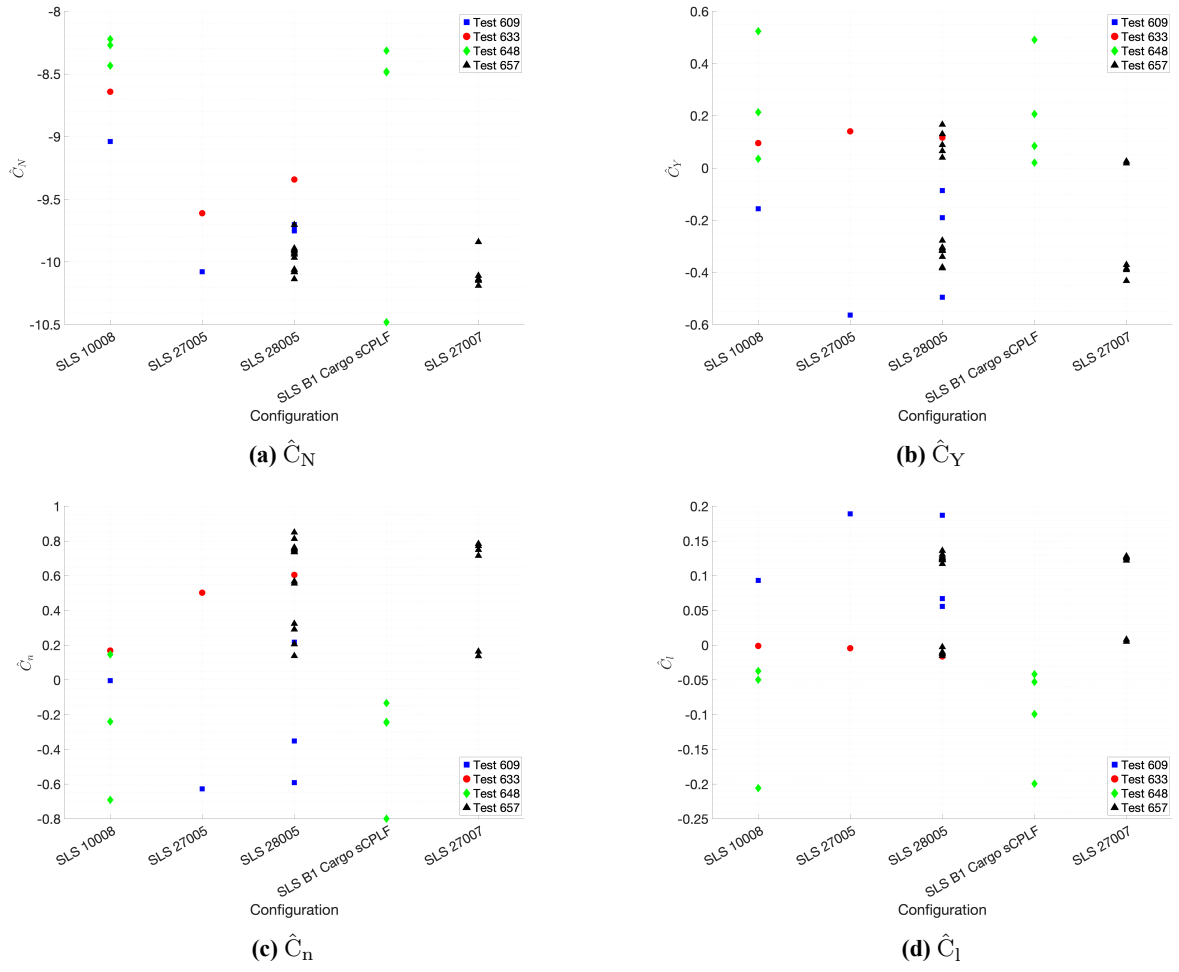

(a) $\hat{\mathrm{C}}_{\mathrm{N}}$ **(b)** $\hat{\mathrm{C}}_{\mathrm{Y}}$

(c) $\hat{\mathrm{C}}_{\mathrm{n}}$ **(d)** $\hat{\mathrm{C}}_{\mathrm{l}}$

Fig. 7 Total vehicle force and moment data across different wind tunnel tests and configurations without ML in tunnel, $\phi_P = 180°$, $h/L = 0$, and $q_\infty = 50$ psf for all cases. Values normalized based on maximum side force and yawing moment on SRBs.

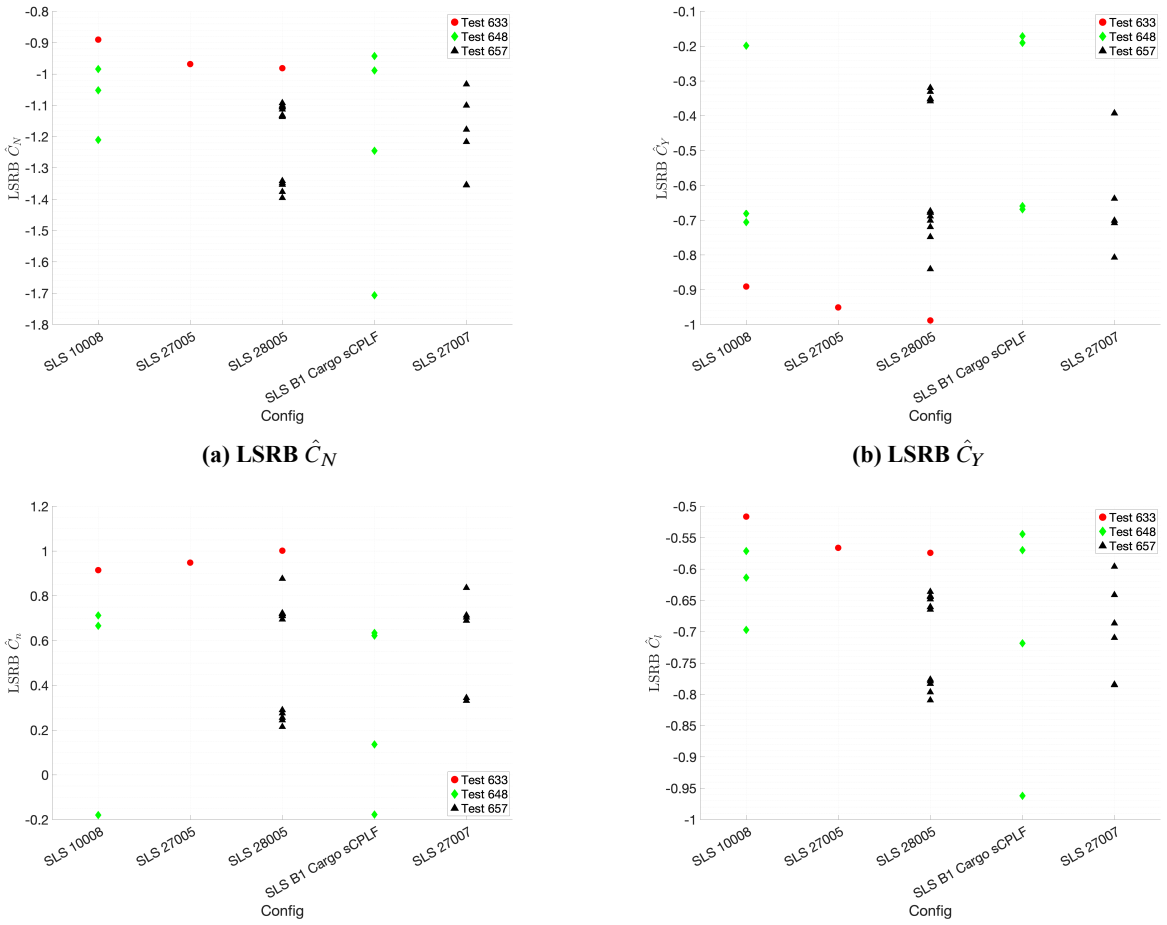

(a) LSRB $\hat{C}_N$ **(b) LSRB $\hat{C}_Y$**

(c) LSRB $\hat{C}_n$ **(d) LSRB $\hat{C}_l$**

Fig. 8 LSRB force and moment data across different wind tunnel tests and configurations without ML in tunnel, $\phi_P = 180°$, $h/L = 0$, and $q_\infty = 50$ psf for all cases. Values normalized based on maximum side force and yawing moment on SRBs.

to conclude anything from Test 609 and Test 633, which is mostly due to a lack of data at the condition of interest in these tests, both of which ran fewer runs in the liftoff configuration and also conducted fewer repeat runs to draw comparisons to. That being said, the data provide a strong case for the existence of multiple stable states potentially caused by the Coandă effect and show the importance of developing alternate methods to account for data at this condition in a lineload or force and moment aerodynamic database.

The LSRB force and moment data are shown in Fig. 8. The data points included are at the same condition as the total vehicle data to allow for direct comparisons to be made. It is important to note that SRB data are not available for Test 609, as the test article did not have fully-instrumented SRBs when this test was conducted. The SRB geometry is the same for all configurations and across all tests and so similar force and moment values are expected for these configurations.

Similar to the total vehicle data, evidence in favor of the presence of a bistable flow state on the LSRB is present in the booster $\hat{C}_Y$. Booster $\hat{C}_N$ also appears to exhibit this bistable trend, although the trend is less noticeable in both $\hat{C}_n$ and $\hat{C}_l$. A lack of data once again restricts drawing any major conclusions from Test 633, but a clear bistable trend is present in the Test 648 data, demonstrating that the Coandă effect has been present across multiple tests and SLS configurations. This behavior is consistent with what has been observed in the CFD and lineloads data, and further emphasizes the need for better targeting of uncertainty when developing a database at this condition.

The RSRB force and moment data are shown in Fig. 9. The condition is the same as the previous two plots, and

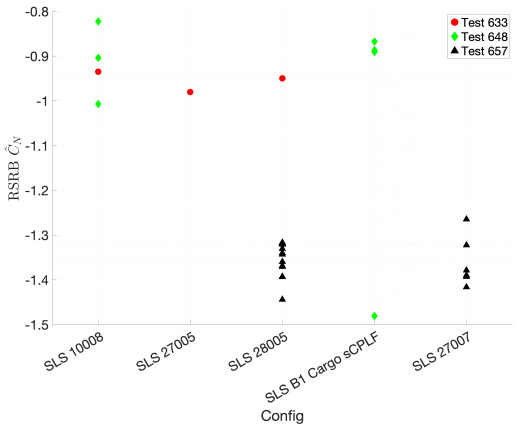

(a) RSRB $\hat{C}_N$

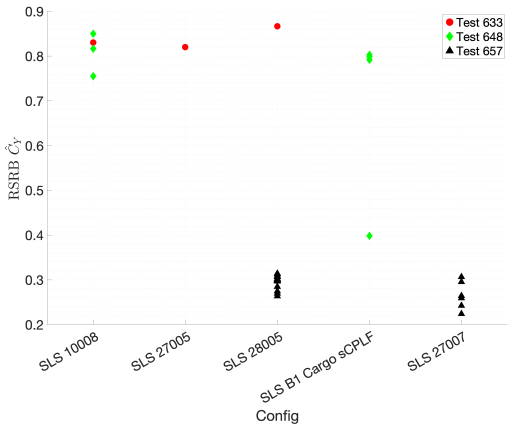

(b) RSRB $\hat{C}_Y$

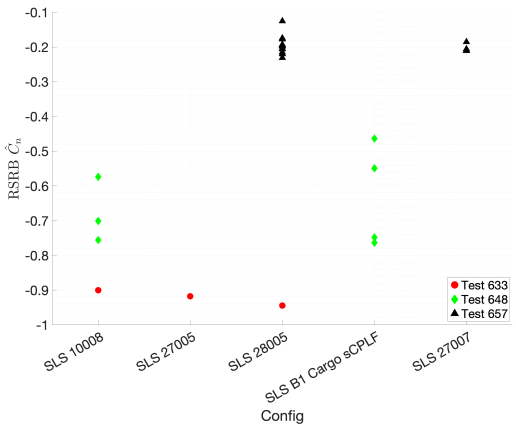

(c) RSRB $\hat{C}_n$

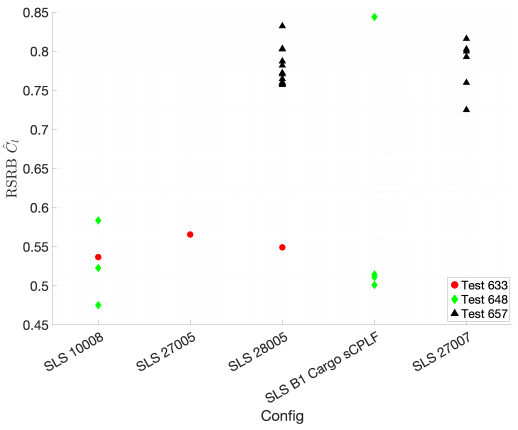

(d) RSRB $\hat{C}_l$

Fig. 9 RSRB force and moment data across different wind tunnel tests and configurations without ML in tunnel, $\phi_P = 180°$, $h/L = 0$, and $q_\infty = 50$ psf for all cases. Values normalized based on maximum side force and yawing moment on SRBs.

SRB data for Test 609 are unavailable. Unlike the total vehicle and LSRB data, the RSRB data do not show as strong a presence of a bistable flow state within tests. There is a slight gap present in $\hat{C}_l$ for Test 657; but outside of this, the data are either tightly bunched around one location or irregularly scattered. With just the time-averaged values, it is impossible to characterize what leads to this scatter. Across tests, however, there is a clear difference between Test 657 and the other two tests in the presented forces and moments. Since the transition grit application of the lower half of the vehicle is constant within a test, it is possible that the applied grit may have a role to play in determining how the flow attaches after passing through the gap between the SRB and the centerbody. However, without more detailed testing to explore this, it is impossible to conclusively show that grit could determine which states are possible.

Because of the difficulty of comparing across the two SRBs in separate plots, Fig. 10 plots the value of $\hat{C}_Y$ for both the LSRB and RSRB against each other. This dataset is expanded slightly from the previous plots to include $h/L \neq 0$ values but is still without the ML. If the only possible values are the extremes of the bistable states, there would be clusters in all four corners, which are defined by the dashed purple lines. As can be seen, there is strong cluster in 3 of the 4 corners and a few points in the top right corner. Since the values are signed, the points along the negative diagonal represent symmetry between the boosters. The four corners are labeled with their respective Coandă state, and is clear evidence that WT testing observed all four states even if there were some states that only occurred a handful of times. There are also a significant number of points that do not fall cleanly into a corner cluster. This is likely due to points that capture either partial states or include state switching during the time averaging window; but without more data, further characterization is impossible.

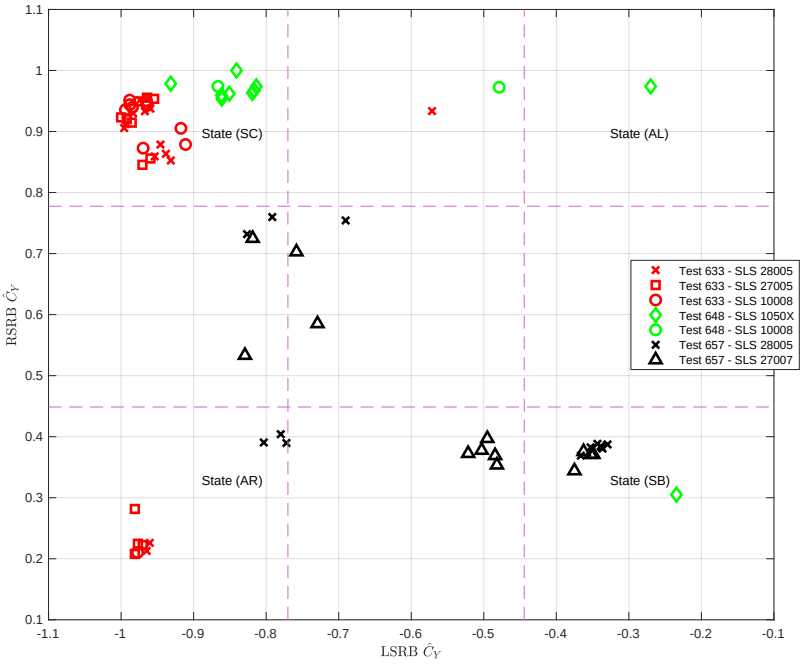

Fig. 10 Plot of $\hat{C}_Y$ for both boosters across different wind tunnel tests and configurations without ML in tunnel, $\phi_P = 180°$, and $q_\infty = 50$ psf for all cases. Values normalized based on maximum side force and yawing moment on SRBs.

The total vehicle force and moment data show that there are at least three stable states. When looking closer at the LSRB and RSRB forces, they each have a bistable state implying the four predicted states; and by plotting their side force values against each other, confirmed which state was present. With these results and the deep dive analysis in the next section, the three states found in the total vehicle can be contributed to the two symmetric states having equal and opposite effects on the individual components. These data are insufficient to categorize which loads are associated with which states and so an examination of more localized flow features is necessary. Static pressure measurements on the centerbody were examined in the hopes of helping to categorize these conditions; however, the small quantity of

static taps and temporal filtering limited the usefulness of these data for identifying the Coandă flow states. Fortunately, the computational results do not have this limitation and can be used to explore more geometrically localized trends.

B. CFD Comparisons

The focus on this subsection is similar to the previous where trends across the collected data are observed to make conclusions about the broader overview. Because of their commonality on the aft portion of the vehicle, computational data from all available configurations of the SLS were gathered. There are a total of 5 configurations represented: Block 1 Crew, Block 1 Cargo, Block 1B Crew, and two version of the Block 1B Cargo. All solutions at α_P = 90° and ϕ_P = 180° are collected with and without the ML present. Simulations at ϕ_P = 0° were also used if the ML was not present and then rotated to line up with ϕ_P = 180°. The data gathered included both database production runs as well as runs used to prototype grid development. This collection of data represent all the computational cases where it is easy to characterize the Coandă effect. This results in about 40 cases of interest across the multiple SLS and ML configurations. After the data were gathered, the lineloads of the three components were plotted together to check for outliers. A few of the prototype grid development cases were removed as outlier due to grid quality issues.

The collection of gathered centerbody lineloads are found in Fig 11. The colors represent various SLS configurations while the solid lines represent cases where the tower was included in the simulation The solid black line is the baseline case used during development of the most recent ground force winds database. It is also highlighted as a representative case of State Symmetric Booster (SB) that will be explored in Section IV.A. On the far left, an outline of the various vehicles can be seen to help line up changes in lineloads to geometric features. In the center are the normal force lineloads and on the right are the side force lineloads. As mentioned previously, these lineloads have all been normalized based on a value to force observed integrated side force on the SRBs to vary between -1 and 1. The cases where the tail service masts are present produce a defect in $\Delta\hat{C_N}/(\Delta\hat{X})$ on the very aft portion of the vehicle but no corresponding change for $\Delta\hat{C_Y}/(\Delta\hat{X})$. There are few patterns to observe here and there are no obvious clustering in either the normal force or side force lineloads to draw conclusions about multimodal behavior. A similar collection of lineloads for the LSRB are found in Fig 12 and finally the RSRB lineloads are found in Fig 13.

Unlike the centerbody, the collection of plotted lineloads on the SRBs clearly show the multiple states possible for the lineloads. For both SRBs, on the constant diameter section, there is a large grouping along $\Delta\hat{C_N}/(\Delta\hat{X})$ = -0.3 and a few about half the value, which show the two states that each SRB may experience. On the side force lineloads, the majority of the cases are at $\Delta\hat{C_Y}/(\Delta\hat{X})$ = 0. Similar to the wind tunnel data, the SRB data are the most informative in regard to observing the existence of the Coandă states. State SB is the most common state observed in the CFD data; however, the bistable state for each SRB is confirmed, which provides more evidence to the predicted four states. Unfortunately, state SC has not been directly observed in the CFD, and conclusions about it must be drawn by inference as is done in the next section.

In the next section, a few highlighted cases will show which state is associated with which lineload clustering and how the surface data change to create each of these lineloads. This analysis is then used to draw conclusions on what to expect for each state.

III. Highlighted In depth Analysis of Coandă States

This section takes a deeper dive into the gathered data to try and characterize how different the lineloads and, as a result, the integrated forces are determined by the Coandă states. The first is an overview of the nominal case, which is currently represented in the recently developed ground wind loads database that required this analysis. The second subsection looks at one of the asymmetric cases and how that asymmetry changes total vehicle forces as well as individual components. The third section examines an observation made possible by the data gathered during Test 657, which shows an interesting lack of relationship between total vehicle normal force and Coandă state. Because of the unpredictability of the Coandă states, State SC was not observed computationally; however, the effects of such a condition can still be predicted, which will be done at the end of this section.

A. Baseline Case: State Symmetric Boosters (SB)

The current work is the result of improving a database for the Block 1B Crew version of the SLS vehicle, and therefore, the CFD solution corresponding to the Block 1B Crew configuration in the presence of the ML-2 with an h/L =0 will be referred to as the baseline case. This case is also representative of the majority of gathered computational data, i.e., State SB is the most commonly observed. Classification is done by examining the magnitude of the coefficient

of friction on the leeward side of the vehicle, as seen in Fig. 14a. These types of plots are the easiest diagnostic method for state determination. In the wind tunnel as discussed later, state determination is harder and requires careful examination of integrated forces.

Figure 14b shows the pressure acting on the windward side of the vehicle while Fig. 14c shows the same data on the leeward side of the vehicle. Note the general symmetry of pressure on the two SRBs. While there are some differences between the two SRBs, in general they have similar features. The combination of the surface friction plot above and the leeward pressure plot show that not only does the Coandă effect increase surface friction, it decreases surface pressure consistent with other examples of the Coandă effect.

These two surface plots are very illustrative but can be difficult to mentally integrate to loadings, which are the metric of interest. Figure 15 shows these surface plots integrated into lineloads. On the far left, an outline of the vehicle is shown, and to the right of that is the normal force lineload. On the far right is the side force lineload. Since this state is symmetric, there are fairly symmetrical loadings on the SRBs as expected. The normal force for both SRBs is almost the same while the side forces are equal and opposite with very minor differences. One thing to note, which will be used in later analyses, is that the side force is mostly zero along the constant diameter section of the SRB. This is a result of balancing of the high pressure region near the gap on the windward side with the low pressure region caused by the Coandă effect.

B. Sample Asymmetric Case: State AR

To help illustrate the effect of a shifting Coandă state, one of the solutions from a similar condition is used. This solution is from a simulation of the Block 1B Crew vehicle in proximity to the ML-1E version of the tower at an h/L = 0.2 at a ϕ_{azi} = 180°. The analysis begins the same way by looking at the magnitude of skin friction to determine the Coandă state. Figure 16a shows that the Coandă effect goes toward the positive Y direction for both gaps. This corresponds to State AR.

The next step is to look at the surface pressure since that is the driving component of forces. Beginning on the windward side, as seen in Fig. 16b, there is significant symmetry similar to the baseline case for State SB. This suggests that any difference between the SRBs is going to be found on the leeward side of the vehicles. Also of note, in comparison to Fig. 14b, the tail service masts are not blocking the flow from impacting the vehicle, which creates a visible difference on the aft portion of the vehicle. The leeward side pressures, as seen in Fig 16c, show the asymmetry expected from this Coandă state. While the region on the centerbody is larger, it has a slightly higher pressure than the corresponding attached region on the SRB. As discussed more thoroughly in Section C using data from the wind tunnel, the region of low pressure and the magnitude are balanced such that the total vehicle normal force is consistent as the Coandă state changes.

Finally, an examination of the lineloads in Fig. 17 is undertaken to better understand the results of this different attachment state. Here, the asymmetry between the SRBs is highlighted both in normal force and side force. The LSRB in blue, which does not have flow attached to it in this state, shows a reduction in normal force that is caused by losing the attached low pressure region found in the nominal case. On the side force, there is now significant force acting away from the centerbody on the LSRB. The changes on the centerbody are harder to quantify but one thing to note is the shift toward the LSRB in the side force. This is caused by the low pressure region on that side of the centerbody. This analysis lets us conclude that the asymmetric states cause increased loading on the total vehicle in the opposite direction of the flow attachments.

C. Coandă State and Normal Force

Due to data gathered during Test 657, a key observation about how the Coandă state impacts integrated forces was possible. Figure 18 shows the integrated forces and moments from two different runs for the total vehicle across an 8 second window. These two runs were selected to show the two different Coandă states picked up at the same conditions during repeat runs. These runs were with the Block 1B Crew in the presence of the ML-2 at h/L =-0.003, ϕ_P = 200°. The dashed lines are the average of the forces and moments while the solid lines are the time varying data. One of these runs, R321 in red, shows the flow briefly flipping between two states as evidenced by Fig. 18c, which shows the side force. Even though the side force clearly changes, indicating Coandă state change, there is no similar change in the normal force. This implies that any change in normal force the SRBs experience is balanced out by a change in the centerbody normal force, which results in the total vehicle having a consistent loading in the normal direction regardless of Coandă state.

D. Changes to Component Loads

From the two sample cases above and the time history data from the wind tunnel, some general characteristics of how lineloads and integrated forces are dependent on the Coandă state are laid out. When the Coandă effect attaches to the SRB, the normal force on the SRB increases due to the resulting low pressure region on leeward side of the SRB. The low pressure region also counteracts the high pressure region that forms on the windward portion of the SRB closest to the centerbody, which results in a very low resulting side force.

When the Coandă effect attaches to the centerbody, the SRB normal force is lower because the leeward side of the SRB no longer has the low pressure region. In contrast, the centerbody now has a low pressure region that in turn increases the normal force on the centerbody. Experimental evidence suggests that this is an equivalent switch and total vehicle integrated normal force remains constant. While the Coandă effect is attached to the centerbody, the SRB side force pushes the component away from the centerbody. The centerbody also tends to be pushed into that same direction due to the suction from the low pressure region. Table 1 summarizes these conclusions and the effect these states have on predicted forces. The values in Table 1b are derived from Fig. 10 and further refinement is possible.

Table 1 Summary of Coandă State Interactions with Integrated Forces.

(a) Absolute value of Normal Force

Component	State SB	State SC	State AR	State AL
Centerbody	Min	Max	Mid	Mid
LSRB	Max	Min	Min	Max
RSRB	Max	Min	Max	Min
Total Vehicle	Nominal	Nominal	Nominal	Nominal

(b) Signed Side Force

Component	State SB	State SC	State AR	State AL
Centerbody	≈ 0	≈ 0	< 0	> 0
LSRB	> -0.45	< -0.75	< -0.75	> -0.45
RSRB	< 0.45	> 0.75	< 0.45	> 0.75
Total Vehicle	≈ 0	≈ 0	< 0	> 0

IV. Conclusions

With this analysis of the Coandă effect on the SLS, the ground wind loads database has been updated to account for the multimodal possibilities. The update focused on providing proper characterization of the side forces and so created alternate nominal values that represent state AR and state AL. While having very different component loads, States SB and SC have similar total vehicle loads. Exact left and right symmetry was not observed in the data, there is little reason to believe that one of the two states should be more common or have significantly different effects. Future expansion of this analysis for the SLS program is likely to focus on what causes the Coandă state to change to determine if the dynamic effects may cause a concern. Observations in the wind tunnel under certain conditions show flipping can happen every couple seconds and so work has continued to explore how to control the Coandă state.

The mechanisms that control Coandă state have yet to be determined, although small scale geometric features may play a role. The applied boundary layer transition grit may be a possible reason why different wind tunnel tests saw different states and points to the "as built" geometry of the SLS influencing what will be observed prelaunch. The application of the thermal protection system during construction results in a final vehicle with many small scale geometric features that are expected like the wind tunnel grit at these conditions. Other methods are likely able to control the resulting Coandă state, but controlling small scale geometry is likely the most direct path forward. Another possibility to control Coandă state is the Reynolds number, which is theorized to play some role in the existence and strength of the jet that forms in the gap flow. The computational results presented are designed to match wind tunnel conditions and so variations of Reynolds number have not been explored. Planned experimental work in the NASA Langley Transonic Dynamics Tunnel and the supporting CFD will incorporate variations in Reynolds number and may provide insight on how the Reynolds number plays a role in determining Coandă state.

This work assumes that the Coandă state is constant along the length of the vehicle but there is some evidence this is not always the case. The computational data on the LSRB in Fig. 12 show a simulation where the state switches part way down the booster. Some of the scatter in the booster integrated forces may also be a result of these partial states, but without more measurements it is impossible to be sure. Future work should start with the assumption that results will not always fall into four states to hopefully give a better understanding on the existence of these partial states. Even though this work focuses on $\alpha_P = 90°$, the Coandă effect has been observed in CFD at midrange α_P (between 30° and 70°); however, these flows become dominated by the asymmetric vortices that form on slender bodies at these conditions [7].

References

[1] Walker, M. A., Pinier, J. T., Shea, P. R., Collins, J. G., Mears, L. J., Lee, M. W., and Pomeroy, B. P., "Experimental Identification of Bistable Flow States on the Space Launch System at Liftoff Conditions," *AIAA Aviation Forum*, 2022.

[2] "Space Launch System," Available at `https://www.nasa.gov/exploration/systems/sls/index.html`, Accessed: 10/15/2021.

[3] *SLS-SPEC-048: Cross-Program Integrated Coordinate Systems*, Revision F.1, 2018.

[4] Krist, S. E., Ratnayake, N. A., and Ghaffari, F., "Kestrel Results at Liftoff Conditions for a Space Launch System Configuration in Proximity to the Launch Tower," *AIAA Aviation Forum*, 2019.

[5] Ratnayake, N. A., Krist, S. E., Ghaffari, F., and Deere, K. A., "Computational Fluid Dynamics Methods Used in the Development of the Space Launch System Liftoff and Transition Lineloads Databases," *AIAA Aviation Forum*, 2019.

[6] Willie, R., and Fernholz, H., "Report on the first European Mechanics Colloquium, on the Coanda Effect," *Fluid Mech.*, Vol. 23, No. 4, 1965, pp. 801–819.

[7] Pomeroy, B. W., and Krist, S. E., "Validation of Kestrel IDDES Simulations for SLS Transition Analysis," *AIAA Scitech Forum*, 2022.

[8] Pinier, J. T., Erickson, G. E., Paulson, J. W., Tomek, W. G., Bennett, D. W., and Blevins, J. A., "Space Launch System Liftoff and Transition Aerodynamic Characterization in the NASA Langley 14x22' Subsonic Wind Tunnel," *53rd AIAA Aerospace Sciences Meeting*, 2015.

[9] Chan, D. T., Paulson, J. W., Shea, P. R., Toro, K. G., Parker, P. A., and Commo, S. A., "Aerodynamic Characterization and Improved Testing Methods for the Space Launch System Liftoff and Transition Environment," *AIAA Aviation Forum*, 2019.

[10] Mears, L. J., Shea, P. R., Collins, J. G., Langston, S. L., Walker, M. A., and Pinier, J. T., "Experimental Characterization of the Space Launch System Block 1B Liftoff and Transition Environment," *AIAA Scitech Forum*, 2023.

[11] McDaniel, D. R., Tuckey, T. R., and Morton, S. A., "The HPCMP CREATE-AV Kestrel Computational Environment and its Relation to NASA's CFD Vision 2030," AIAA Paper 2017-0813, AIAA SciTech Forum, Grapevine, TX, 2017.

[12] McDaniel, D. R., and Tuckey, T. R., "HPCMP CREATE-AV Kestrel New and Emerging Capabilities," AIAA Paper 2020-1525, AIAA SciTech Forum, Orlando, FL, 2020.

[13] Morton, S. A., and Meakin, R. L., "HPCMP CREATE-AV Kestrel Architecture, Capabilities, and Long Term Plan for Fixed-Wing Aircraft Simulations," AIAA Paper 2016-0565, AIAA SciTech Forum, San Diego, CA, 2016.

[14] Morton, S. A., McDaniel, D. R., Sears, D. R., Tillman, B., and Tuckey, T. R., "Kestrel - A Fixed Wing Virtual Aircraft Product of the CREATE Program," AIAA Paper 2009-338, AIAA Aerospace Sciences Meeting, Orlando, FL, 2009.

[15] Ratnayake, N. A., Krist, S. E., and Ghaffari, F., "Selection of Computational Fluid Dynamics Tools Used in Development of the Space Launch System Liftoff and Transition Lineloads Databases," AIAA Paper 2019-1840, AIAA SciTech Forum, San Diego, CA, 2019.

[16] Pomeroy, B. W., Krist, S. E., Wignall, T., Lee, M. W., Ghaffari, F., Deere, K. A., Collins, J. G., Ratnayake, N. A., Streett, C. L., Goushcha, O. O., Vogel, E. A., and Pinier, J. T., "NASA Langley Low-Speed CFD Contributions to the Space Launch System Program," AIAA Paper 2023-XXXX, AIAA SciTech Forum, National Harbor, MD, 2023.

[17] Gentry, C. L., Quinto, P. F., Gatlin, G., and Applin, Z., "The Langley 14- by 22-Foot Subsonic Tunnel: Description, Flow Characteristics, and Guide for Users," 1990, NASA-TP-3008.

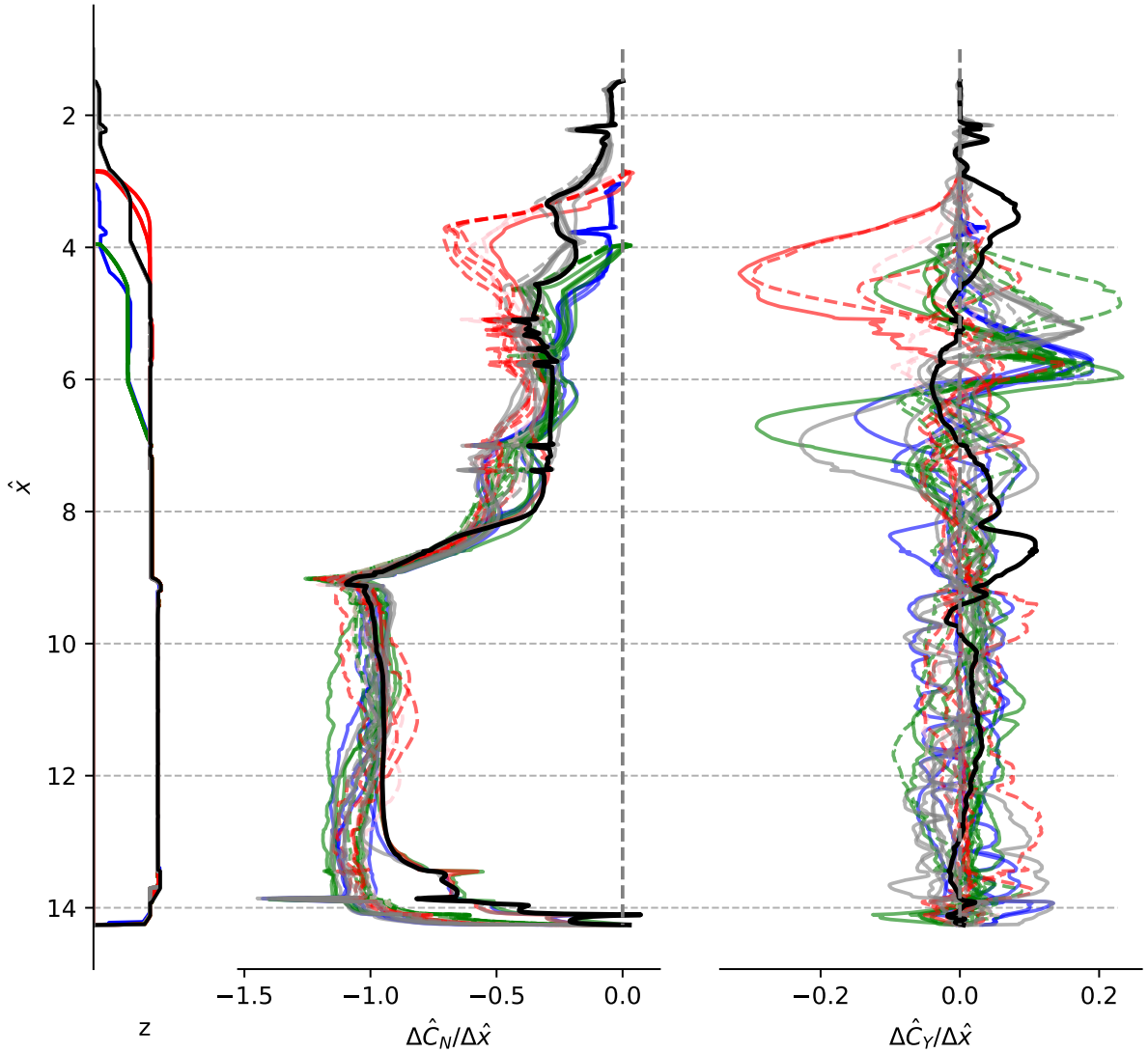

Fig. 11 Lineloads on the centerbody. Colors represent various SLS configurations, dashed lines are from simulations without the ML. Values normalized based on maximum integrated side force and yawing moment on SRBs.

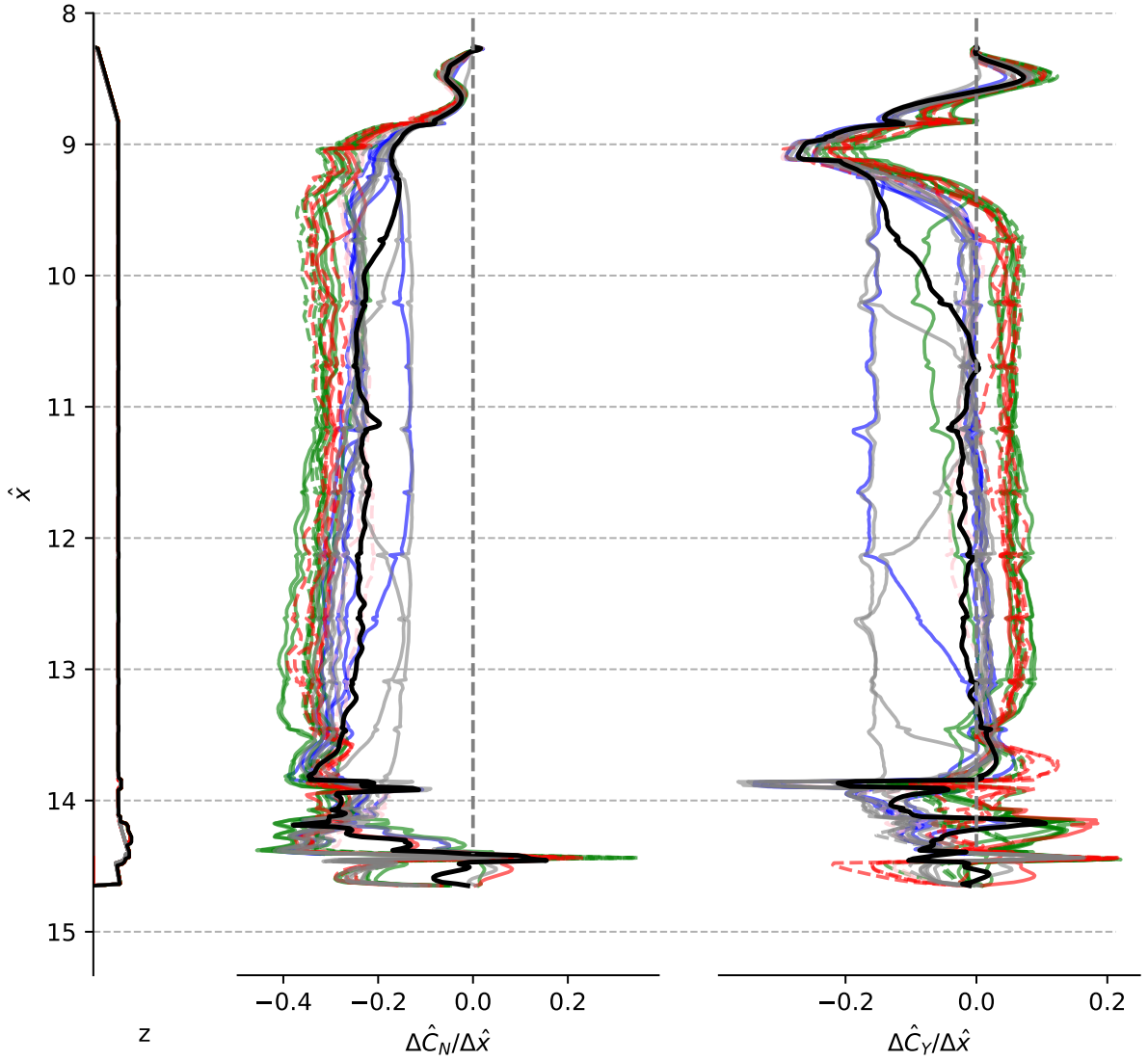

Fig. 12 Lineloads on the LSRB. Colors represent various SLS configurations, dashed lines are from simulations without the ML. Values normalized based on maximum integrated side force and yawing moment on SRBs.

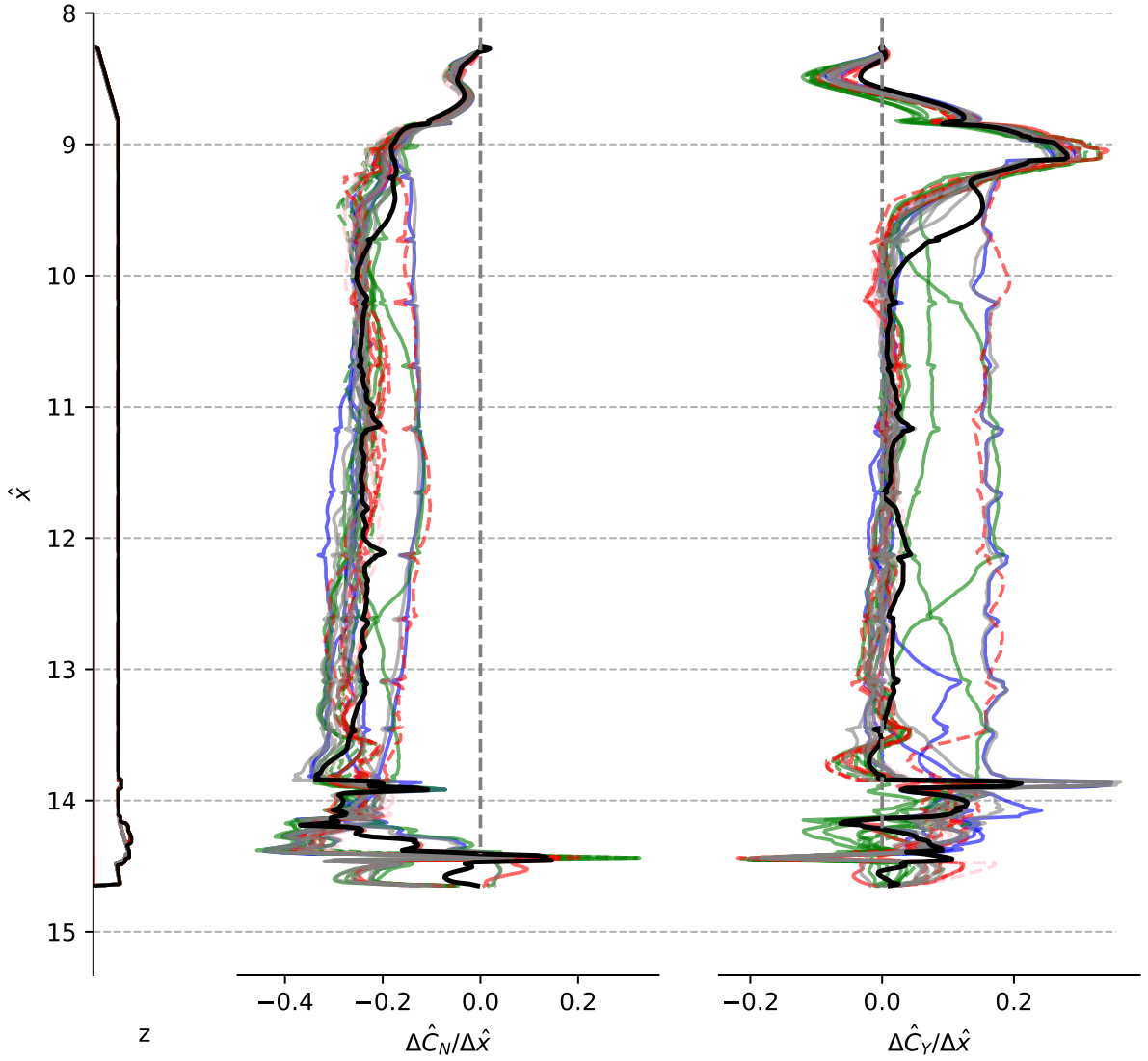

Fig. 13 Lineloads on the RSRB. Colors represent various SLS configurations, dashed lines are from simulations without the ML. Values normalized based on maximum integrated side force and yawing moment on SRBs.

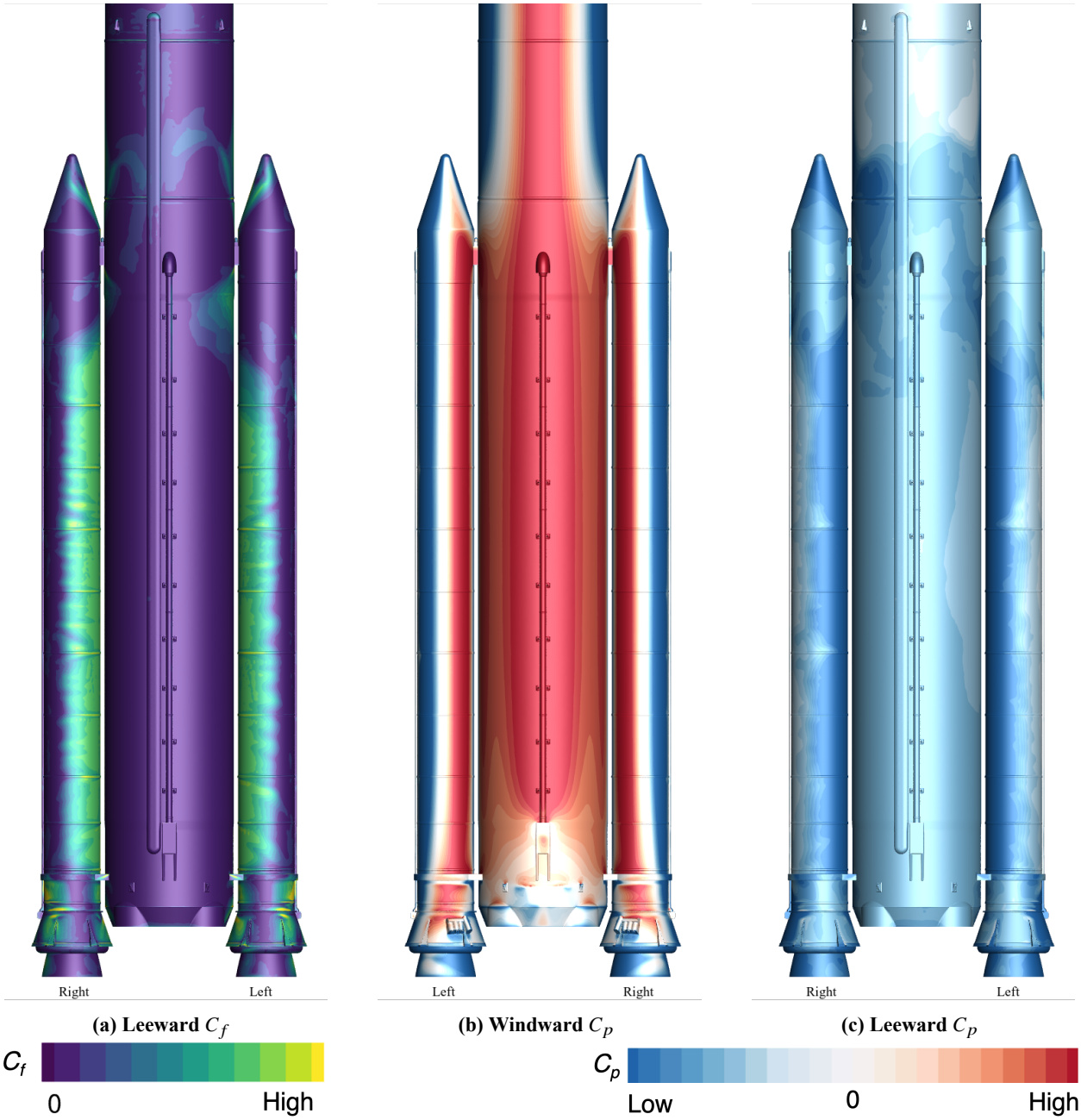

(a) Leeward C_f **(b) Windward C_p** **(c) Leeward C_p**

Fig. 14 Time-averaged surface data of the Block 1B Crew at h/L= 0, ψ_{azm} = 180° in proximity to the ML-2. (a) The skin friction C_f on the leeward side showing attached flow to both SRBs, (b) C_p on the windward side showing symmetry between the SRBs, and (c) C_p on the leeward side showing the region of lower pressure on both SRBs caused by the Coandă effect.

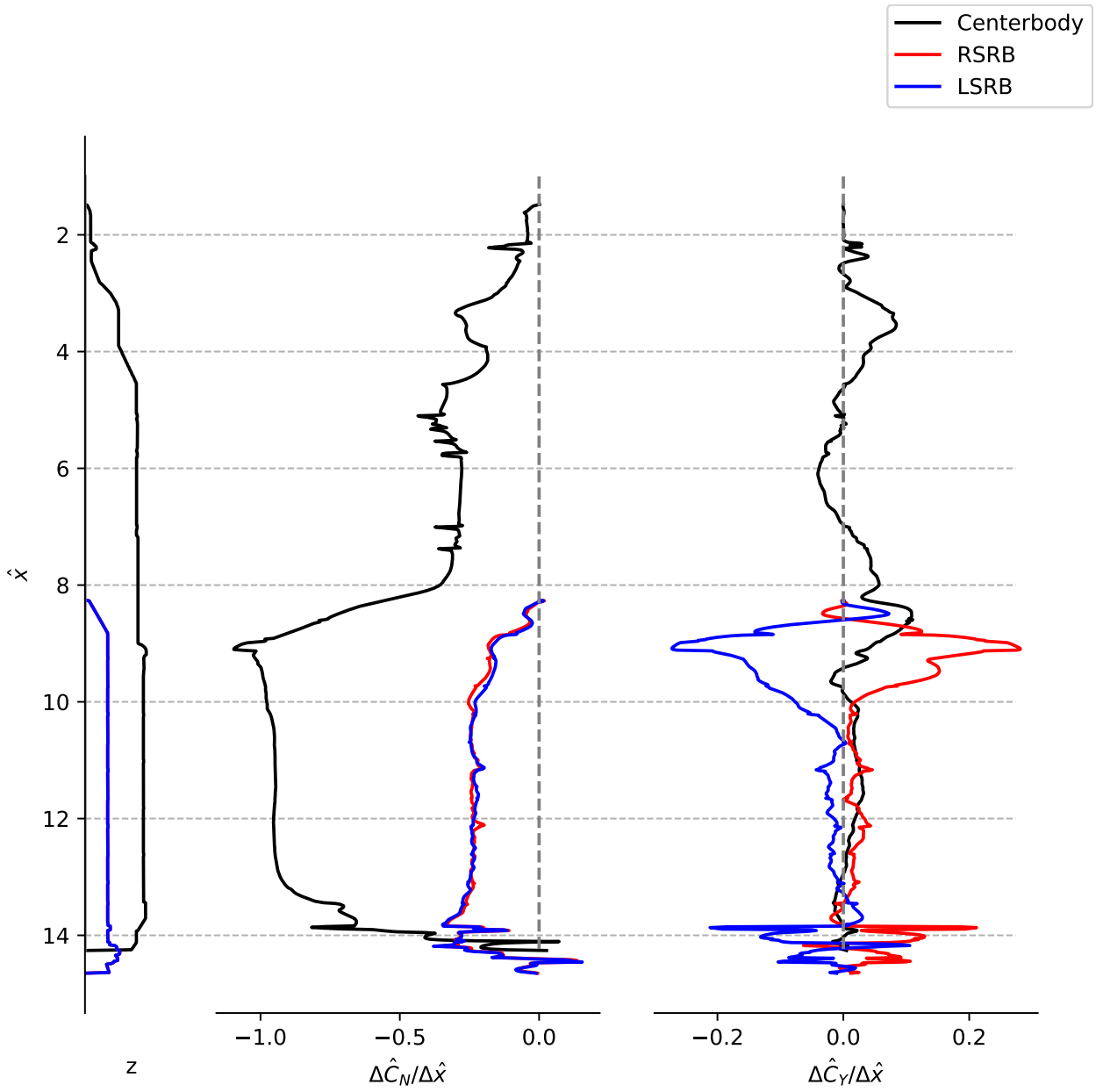

Fig. 15 Lineloads for the baseline case, which is a representative example of State SB. The symmetric Coandă state causes symmetric loading on the SRBs. Values normalized based on maximum side force and yawing moment on the SRBs.

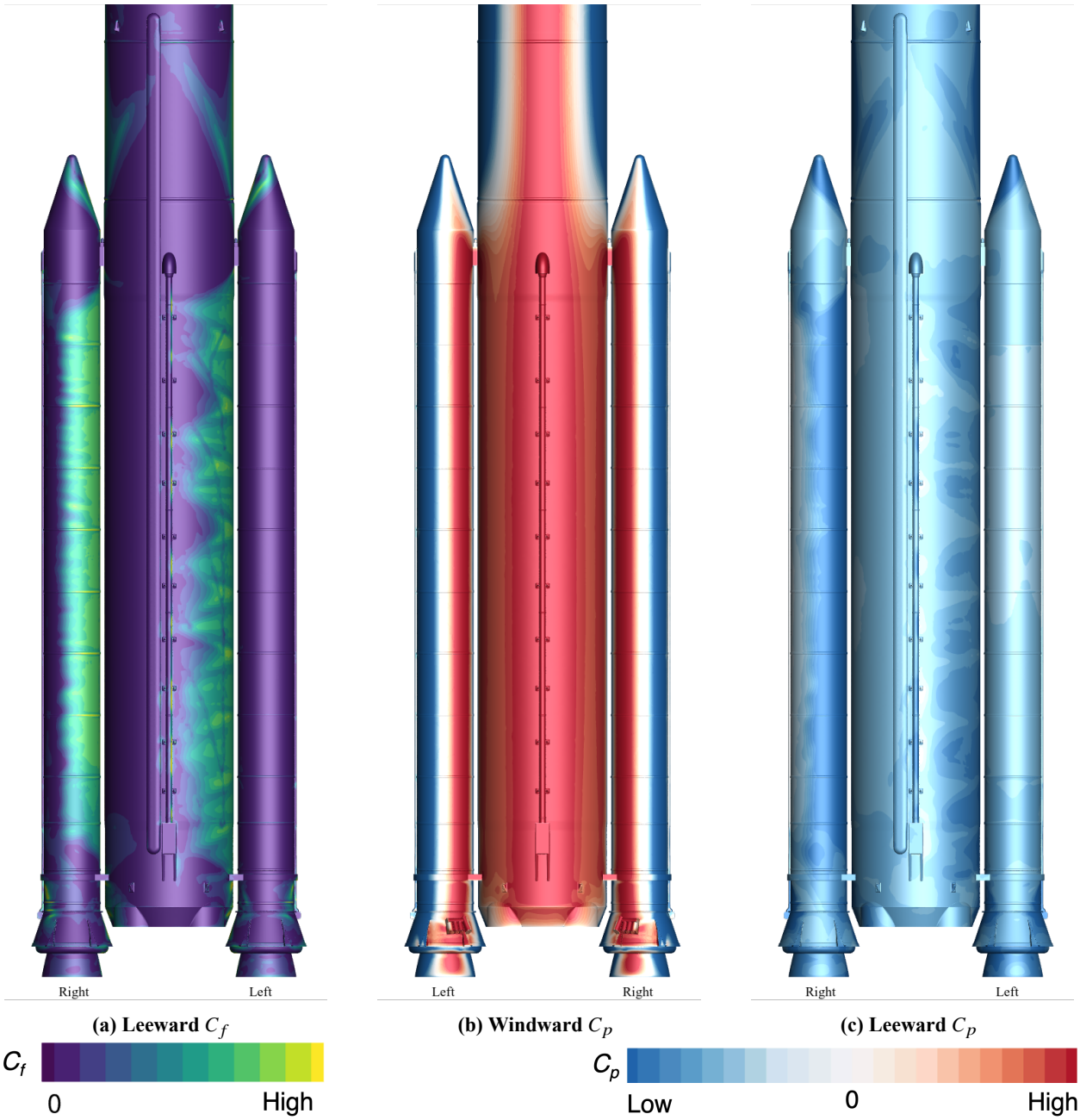

(a) Leeward C_f **(b) Windward C_p** **(c) Leeward C_p**

Fig. 16 Time-averaged surface data of the Block 1B Crew at h/L= 0.2, ψ_{azm} = 180° in proximity to the ML-1E. (a) The skin friction C_f on the leeward side showing attached flow on the RSRB and the left side of the centerbody, (b) C_p on the windward side showing symmetry between the SRBs, and (c) C_p on the leeward side showing the region of lower pressure on the RSRBs and the left side of the centerbody caused by the Coandă effect.

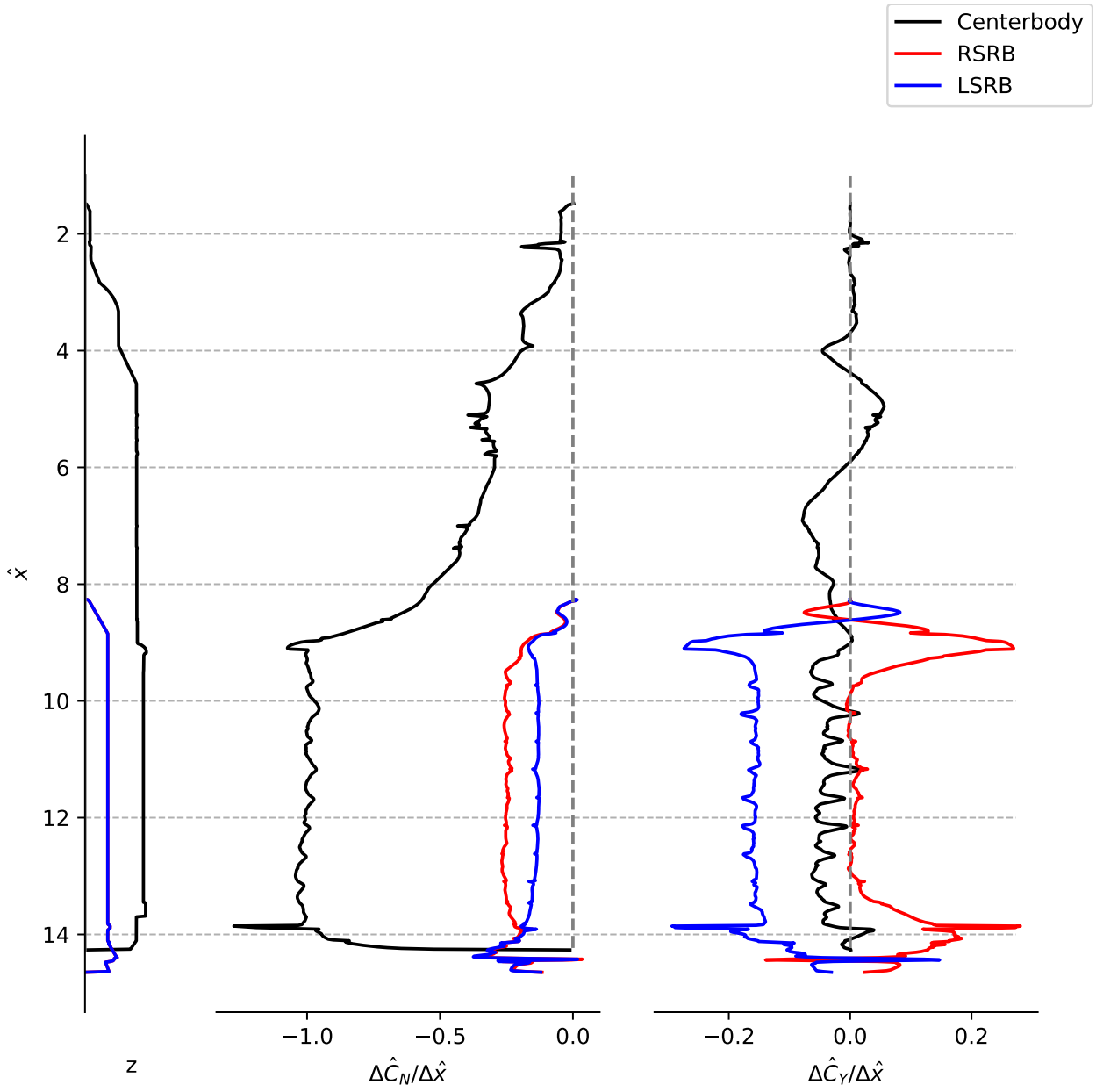

Fig. 17 Lineloads for a simulation at State AR. Values normalized based on maximum side force and yawing moment on SRBs.

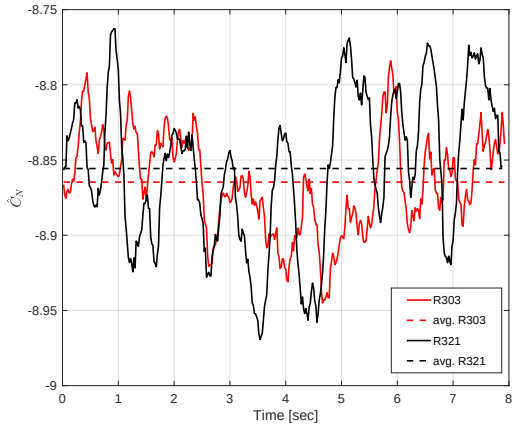

(a) C_N

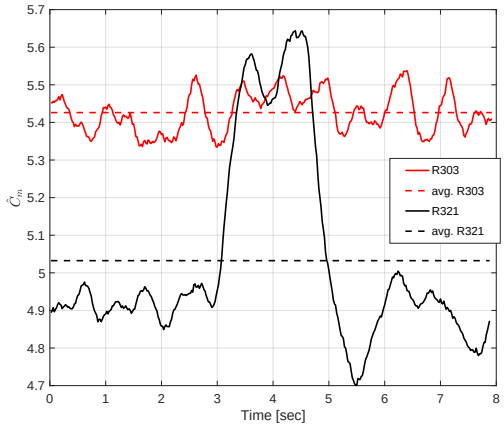

(b) C_m

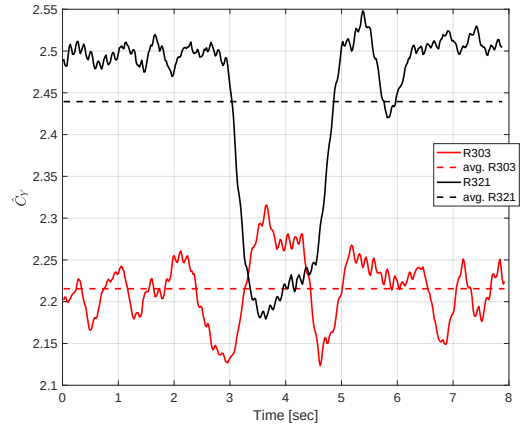

(c) C_Y

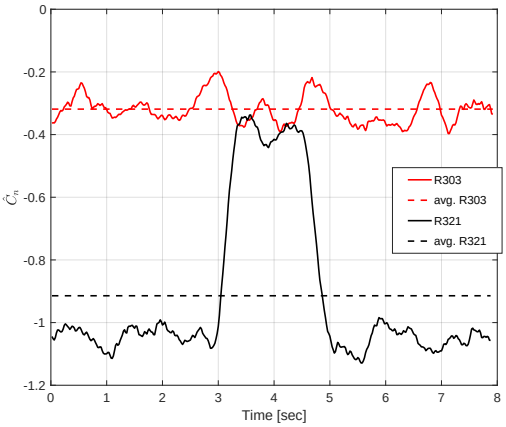

(d) C_n

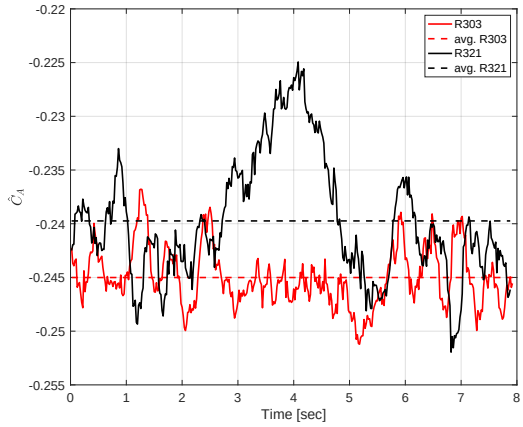

(e) C_A

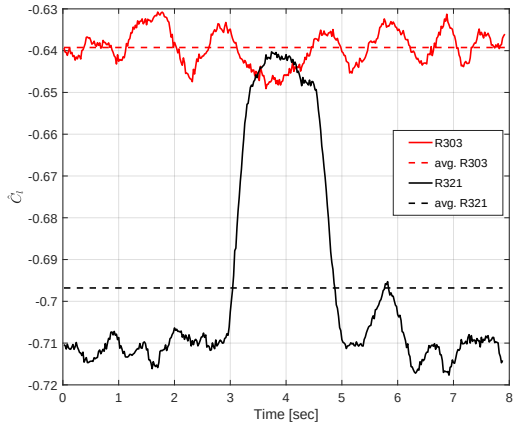

(f) C_l

Fig. 18 Time-dependent total vehicle force and moment coefficients, SLS Block 1B Crew, ML-2 installed, ϕ_P = 200°, h/L = -0.003, q_∞ = 50 psf [1].